Performance, Combustion and Emissions Evaluation of Liquid Phase Port-Injected LPG on a Single Cylinder Heavy-Duty Spark Ignited Engine

Toluwalase Fosudo, Tanmay Kar, Bret Windom, Jacob Schlagel, and Daniel Olsen
Colorado State University

Abstract

Liquefied petroleum gas (LPG), like many other alternative fuels, has witnessed increased adoption in the last decade, and its use is projected to rise as stricter emissions regulations continue to be applied. However, much of its use is limited to dual fuel applications, gaseous phase injection, light-duty passenger vehicle applications, or scenarios that require conversion from gasoline engines. Therefore, to address these limitations and discover the most efficient means of harnessing its full potential, more research is required in the development of optimized fuel injection equipment for liquid port and direct injection, along with the implementation of advanced combustion strategies that will improve its thermal efficiency to the levels of conventional fuels. This paper focuses on the development of a liquid phase port-injection system for LPG, the design of a reference piston, and the baseline evaluation of the performance, combustion, and emissions characteristics of a single cylinder research engine to establish a benchmark comparable to existing LPG engines. A sweep of start of injection (SOI) timing is performed by injecting liquid LPG at several closed and open intake valve timings, which demonstrates no significant variation in engine performance, but accounts for a 10% reduction in bsCO with the optimal SOI timing. Spark timing sweep demonstrates the 50% burn crank angle location related to maximum brake torque (MBT) point with a brake thermal efficiency (BTE) of ~34% for the tested load case. The effect of equivalence ratio is also presented with optimal SOI timing at MBT condition. The engine starts exhibiting knocking combustion at 140kPa intake manifold air pressure (IMAP) with a peak torque of 253Nm and a 5% reduction in brake specific fuel consumption compared to the naturally aspirated scenario.

Introduction

Alternative fuels such as compressed natural gas (CNG), liquefied petroleum gas (LPG), and biofuels currently account for over 10% of the total energy consumed in the transportation sector, and this figure is projected to increase for the next 30 years [1]. The major driving force behind this increased adoption is their potential for substantial emission reductions, while the biggest drawback is the engine compatibility and level of investment in infrastructures that would be required to maximize the potential of these fuels [2, 3]. In the heavy-duty sector, heavier liquid fuels dominate [3] with their contribution to transportation energy consumption estimated to be around 25% [1]. LPG, a relatively lighter fuel, has the key physical advantage of being easily liquefied at moderate pressures and, therefore, the existing infrastructure can be utilized for its transport, storage, and handling, thus requiring less initial investment for its use in the transportation sector [3] making it an attractive, cheaper immediate option in the energy transition. Chemically, LPG consists mostly of propane, butane, and propylene, each in varying amounts determined by several factors including the refining process, the balance of demand for the various refined products, and season [4]. In Europe, EN 589 puts a limit on LPG blend properties, not its composition [4], while the HD-5 specification exists in the US which limits LPG propylene content to less than 5% and requires at least 90% propane [5]. This variation in LPG composition generally affects its properties and performance [4, 6-7].

LPG has found increased relevance in spark ignition (SI) engine applications due to its high knock resistance and is positioned at the forefront of viable alternative fuel option for heavy-duty SI applications [8-9]. Boretti et al. [10] estimated that nearly 40% of refueling outlets supplied LPG, the dominant alternative fuel in Australia, with over half a million vehicles on the road as far back as 2002. Lasocki et al. [11] investigated the use of LPG in a range extender and showed fewer CO_2 emissions and comparable levels of brake specific fuel consumption (BSFC) than the baseline gasoline operation. Nutu et al. [12] demonstrated a ~25% reduction in oxides of nitrogen (NOx) and 20% reduction in BSFC for a dual fuel application with 25% diesel fuel substitution by LPG. The application of LPG in dual-fuel systems to produce lesser CO_2 emissions and regulated pollutants is also documented [13]. As part of a custom fuel blend, a direct injected (DI) diesel blend with LPG as one-third of its mass fraction resulted in a 50% reduction in smoke emissions [14]. One study with LPG-acetylene blends in an SI engine over different relative air to fuel ratios indicated low CO emissions especially during lean operation but observed a substantial increase in NOx emissions [15]. Studies investigating the effect of gaseous phase LPG injection on engine performance showed a considerable drop in performance compared to gasoline due to a loss of volumetric efficiency [4, 16, 17]. Pradeep et al. [18] modified a 2-stroke manifold injected gaseous LPG SI engine to run on direct injected gaseous LPG and showed a significant improvement in the thermal efficiency and up to 93% reduction in HC emissions. Generally, gaseous LPG promotes mixing, improves the rate of combustion, and contributes to lower hydrocarbon and carbon monoxide emissions compared to conventional fuels [18-20].

Although it has been shown that gaseous phase LPG injection is advantageous for the mixing process, the volumetric efficiency drawbacks of these systems can be avoided by the utilization of liquid phase port-fuel and direct injection (DI). Watson et al. [17] compared results from liquid and gaseous phase port injection in a single cylinder engine (SCE) which showed the liquid LPG PFI system had a 2-4% higher thermal efficiency than the gaseous LPG system before getting to the lean misfire limit. Tukiman et al. [21] retrofitted a 1.6L engine with a port-injected, liquid sequential injection (LSI) LPG system and showed a significantly lower BSFC and CO but slightly higher NOx emissions compared to gasoline operation. The combustion parameters of a lean burn DI LPG engine with a spray-guided system were studied by Park et al. [22], and their findings showed that retarded fuel injection would produce favorable conditions for efficient combustion in this DI mode. Dube et al. [23] conducted experimental studies on a 2-stroke SI engine with DI

liquid LPG and compared its performance with liquid phase manifold injected LPG; results showed about 4% improvement in thermal efficiency and a significant effect of the end of ignition (EOI) timing on BTE, HC, and NO emissions. The development of specialized liquid phase LPG injectors enables higher pressure injection, finer atomization of the sprays, charge cooling, and generally accounts for a significant increase in efficiency, but the hardware is complex to develop due to the LPG fuel properties which can cause unwanted vaporization, bubble formation, and cavitation [10, 20, 24]. Recent studies have endeavored to tackle this complexity and have described the development and experimental investigation of liquid phase LPG direct injection systems. Tuan et al. [25] suggested adding a heating element to prevent freezing of the liquid LPG injector tip with fine control of the tip temperature to also avoid strong evaporation that may result in decreased injection amount. A fuel delivery system utilizing a prototype LPG DI injector modified from a gasoline direct injector for use on the heavy-duty Cummins engine was developed to supply liquid LPG at around 17.2MPa, initial tests showed the prototype injector produced higher injection flow rate than the stock injector [24]. In addition, there have been attempts to demonstrate the effectiveness of alternative fuels in heavy-duty applications, however, most of these works are in dual fuel applications, with LPG-diesel/gasoline blends or with natural gas as the single fuel [14, 26-29]

Therefore, extensive research is still required to position LPG as a choice fuel for heavy-duty engines. The purpose of this paper is to demonstrate the successful application of liquid LPG port-injection on a heavy-duty engine and establish a set of baseline test data with which to compare future improvements that will be made possible as advanced combustion strategies are applied on the engine. This study is the first phase of a much broader research that seeks to address the principal shortcomings that prevent heavy duty on-road LPG engines from achieving near-diesel efficiencies e.g., knock [30]. As such, a particular area of interest in the broader research is the characterization of LPG knock, and the expansion of the knock limit. Knock is an abnormal combustion phenomenon [31] where the compressed gas mixture ahead of the flame front auto-ignites and causes pressure oscillations within the combustion chamber. Numerous studies have been dedicated to understanding this phenomenon, underlining its significance in engine research. For LPG knock, Fosudo et al. [6] studied the effect of LPG composition on knock in a CFR engine, Kar et al. [32] performed numerical and experimental investigations into the effect of EGR and fuel composition on a premixed SI engine while Krieck et al. [9] studied pre-ignition and knock on a DI SI Ford engine with various LPG formulations. This paper first describes the test set up: a 15L heavy-duty Cummins engine modified to a single cylinder engine (SCE), then the design of the liquid LPG port injection system along with the design of a reference 9.3:1 piston to mimic the performance of a current LPG engine on the market, the Roush Cleantech Ford 6.8L-V10; which is certified to ultra-low emissions limits, but falls short when compared with the typical diesel engine fuel economy [30]. Finally, a parametric study is done with ignition timing, load, phi, and start of injection (SOI) sweeps to determine the best performance of the engine, quantify its engine-out emissions, and determine its combustion behavior and knock limits. The results indicated an optimal combustion phasing for the engine operation on LPG, consistent liquid LPG injection with the fueling system, excellent control of the air-fuel ratio and the combustion in the engine, and the potential for increasing the brake thermal efficiency while reducing fuel consumption and emissions.

Experimental Set-up

The four key components used for this study were: the single cylinder research engine derived from a Cummins X15 multi-cylinder engine, the liquid phase port-fuel injection (PFI) system, the baseline piston, and the exhaust gas sampling and measurement equipment. This section provides a description of these components, the relevant analysis methods that were deployed in the study and the key assumptions that were made.

Single Cylinder Engine (SCE) Test Cell

The single cylinder engine used in this study was a converted Cummins ISX15L 6-cylinder diesel engine. The conversion involved replacing five of the six original pistons with carefully machined dummy pistons to provide balance on the crankshaft as the active piston, the piston in cylinder number 6 in this case, was operated. The cylinder head was modified to accommodate a spark plug in the location originally intended for the diesel direct injector. The turbocharger, fuel pump, exhaust gas recirculation (EGR) components, and other diesel-allied components were also uninstalled from the original engine. The SCE is water-cooled and has the capability to run at higher loads using compressed air from the research facility. A friction model which was based on an analysis of the production diesel engine was used to account for the other cylinders thus allowing brake mean effective pressures to be calculated from the indicated mean effective pressures. Exhaustive details of the conversion and required modifications that were carried out on the original ISX15 diesel engine can be found in the experimental studies done by Rodriguez et al. [29]. A detailed specification of the SCE is presented in Table 1.

Table 1. The single cylinder engine specifications.

Displacement volume (L)	2.5
Stroke (mm)	169
Bore (mm)	137
Connecting Rod (mm)	261.5
Compression ratio	9.3:1
Number of Valves	4
Exhaust Valve Open	19° BBDC
Exhaust Valve Close	2° BTDC
Inlet Valve Open	11° BTDC
Inlet Valve Close	155° BTDC

Apart from the modifications that were made to the engine hardware, several upgrades were made to the SCE and its test cell to facilitate the collection and analysis of combustion data, and determination of the performance of the engine under different operating conditions. In-cylinder pressure measurements were made with an AVL GH14DK pressure transducer (range 0-300bar) installed in the active cylinder. High speed manifold pressure measurements were performed using a Kistler 4007D piezoresistive pressure transducer and a water-cooled Kistler 4049B piezoresistive pressure transducer for intake and exhaust pressures, respectively. A BEI H25 series encoder with 0.1 crank angle resolution and LabView based high-speed National Instrument hardware (NI PXIe 6363) were used to record and analyze combustion and manifold pressure signals. A Woodward large engine control module (LECM) was used to control injection, ignition, combustion, and air-fuel ratio while giving real-time updates on the state of combustion in the cylinder. The LECM

received a lower resolution position signal using a hall effect crank sensor. A model of the original X15 engine showing the converted single cylinder is shown in Figure 1.

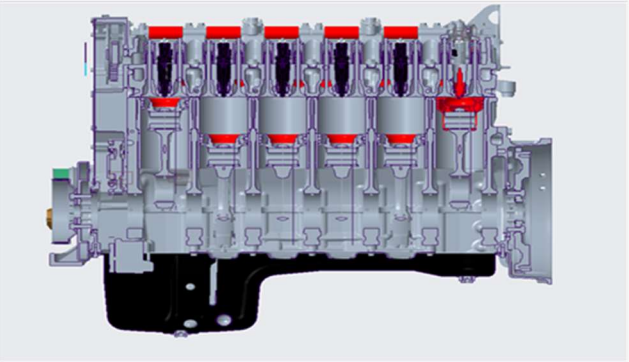

Figure 1. A CAD model of the X15 engine showing the 5 deactivated cylinders and the rightmost cylinder with the spark plug installed.

Key performance parameters were also recorded on LabView software platform using the NI 6224 and 6704 modules and on the LECM. These measurements include fuel flow rate measured using a Bronkhorst M15 Coriolis flow meter, air-fuel ratio measured with a wide-band lambda sensor LSU 4.9 (application range: lambda 0.65 to ∞), and pressure and temperatures measurements made at the required locations using absolute pressure transducers and K-type thermocouples. The engine speed was controlled by an Eaton SVX variable frequency drive (VFD) which turned the engine during motoring and applied a load during combustion. This VFD was controlled by LabView, and its value recorded in LabView as well. The high-speed combustion and manifold pressure data were logged for 1000 cycles, while 200 cycles of combustion data were logged on the LECM. Other parameters such as the fuel flowrate, engine speed, and fuel pressure were logged at a slower rate of 2Hz for 2 minutes.

Baseline Piston

A 9.3:1 compression ratio (CR) baseline piston was designed with CAD software and was fabricated at the research facility using a 3-axis computer numerical control (CNC) milling machine. The 9.3:1 CR piston was chosen to enable the baseline operation of the SCE on liquid LPG described in this paper replicate the performance of current LPG engines. Two of such identified LPG engines currently on the market are the Power Solutions International 8.8L-V8 engine and the Roush Cleantech Ford 6.8L-V10, used in the Navistar 44 CE Series and Blue Bird school buses, respectively. These engines have compression ratios of 9.1:1 and 9.2:1 respectively. A blank stock piston with the required cooling gallery was provided by Cummins and then machined to achieve 9.3:1 CR. Cummins also provided technical assistance on the minimum recommended piston crown and bowl thickness for an assumed maximum peak pressure of 7MPa. The target brake mean effective pressure (BMEP) to match the Blue Bird LPG engine at naturally aspirated conditions was 900kPa. The 9.3:1 CR was achieved by milling material off the blank piston to obtain the required clearance volume (Vc) shown in Equation 1.

$$Vc = \frac{Vd}{(CRt - 1)} \tag{1}$$

Where:

Vd is the displacement volume = 2.49 x 10^{-6}mm^3

CRt is the target compression ratio = 9.3

Figure 2 shows the CAD model of the final 9.3:1 CR piston.

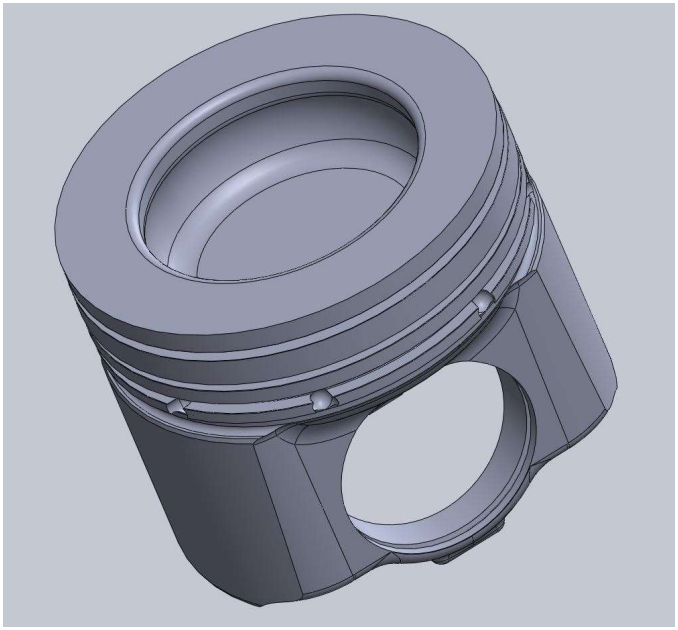

Figure 2. A CAD model of the baseline 9.3:1 piston used in this study.

Port Fuel Injection (PFI) System

The fuel injection system in Figure 3 was designed to ensure a steady supply of liquid LPG to an injector just upstream of the intake valve on the SCE, without any valve targeting. The LPG injector used in this study was the Siemens DEKA injector also used on the Roush Cleantech Ford 6.8L-V10 engine. The high impedance injector was controlled by the LECM and delivered the required amount of liquid fuel at all operating conditions. The liquid fuel delivery system consisted of a high-pressure nitrogen cylinder connected to the vapor port of an LPG tank. The nitrogen enters the LPG tank, through two sets of pressure regulators, at a pressure of ~1.6MPa. Several studies have shown that this pressure is sufficiently above the LPG vapor pressure to ensure liquid LPG all through the system [33, 34].

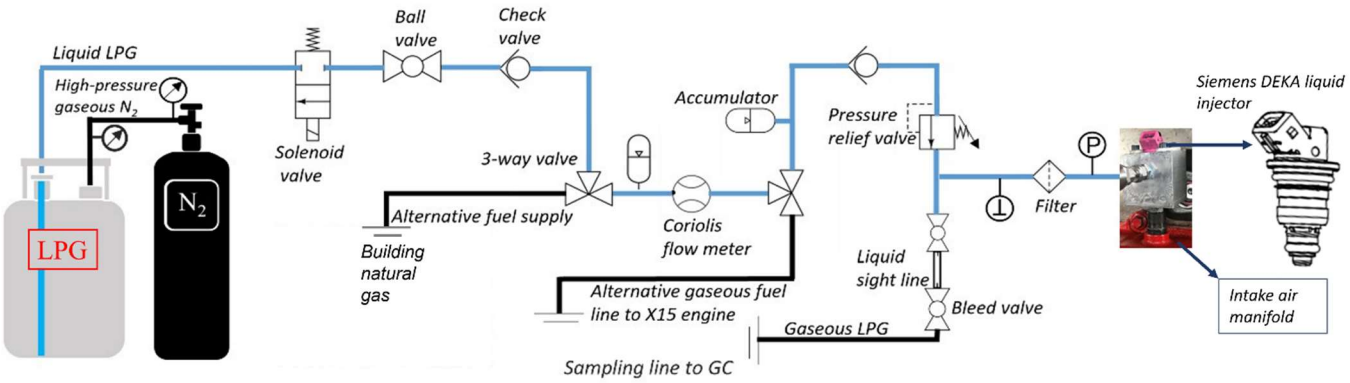

Figure 3. The schematic of the PFI system.

The system was designed in such a way that it incorporated the possibility of alternative fueling options on the SCE with a 3-way valve installed just upstream of the Coriolis flow meter. Two accumulators were installed up and downstream of the Coriolis flow meter to dampen any pressure fluctuations and ensure a reliable fuel flow rate measurement with the flow meter. Density measurements were displayed by the visual interface of the Coriolis flow meter, and this was a useful tool to confirm the state of the LPG in the fuel line. A sight tube installed upstream of the engine also provided visual confirmation of the phase of the fuel. Finally, pressure and temperature measurements were made just before the injector to determine the injection pressure, and as a final check on the thermodynamic state of the fuel entering the injector. Downstream of the liquid sight tube and bleed valve, the fuel line was connected to an INFICON Micro GC Fusion 2-module system gas chromatograph to give the real-time composition of the fuel entering the injector. As the system involved nitrogen and Battino et al. [35] showed that nitrogen was soluble over time in LPG, particular care was taken to eliminate this possibility in this work. The empty LPG tanks were completely purged of the nitrogen gas before each refill and nitrogen contact time with the LPG minimized by only initiating the flow of the gas into a freshly filled LPG tank at the beginning of the test day. These methods were successful as the gas chromatographs showed a negligible amount of nitrogen in the fuel samples.

Exhaust Sampling

Exhaust gas composition was measured using two exhaust sampling equipment by passing the gas through a heated line connected to the tail pipe. These were a Rosemount 5-gas emissions bench analyzer from Siemens Instruments which measures CO, CO_2, THC, NOx and O_2, and an MKS Instruments Fourier transforms infrared (FTIR) spectrometer which measures hazardous air pollutants and other compounds of interest. The 5-gas analyzer includes a condenser component which removes water from the exhaust sample and outputs dry emission measurements. A detailed description of both equipment can be found in the research work done by Fosudo et al., [6]. In order to capture NMHC and for consistency, only the MKS spectrometer results were presented in this work; however, the outputs were checked against the 5-gas analyzer output for verification. Methods developed by Urban et al., [36] described the calculation of the air-fuel ratio using exhaust gas composition. Equations 2 - 4 from their work were applied to calculate the equivalence ratios in this study, and all stoichiometric conditions agreed to within 1% with the equivalence ratios output from the wide band lambda sensor used on the engine. This pointed to an excellent control of the air-fuel ratio and the accuracy of fuel flow and exhaust measurements at all these conditions.

$$H2FAC = \frac{0.5 * y * (\%CO) * (\%CO + \%CO2)}{(3.5 * (\%CO2) + \%CO)} \quad (2)$$

$$A = 0.25 * y - 0.5 * z + \cdots + \frac{\%CO2 + ((0.5 * z) - 0.25 * y) * \%HC + 0.5 * \%CO + .5 * \%NOx + \%O2 - 0.5 * H2FAC}{\%CO2 + \%CO \quad \%HC} \quad (3)$$

$$AFR = \frac{138.28 * A}{12.011 + 1.008 * y + 15.999 * z + 14.008 * f} \quad (4)$$

For the fuel $C_xH_yO_zN_f$

Where:

AFR = Air-fuel ratio

x = 1

H2FAC is the computed exhaust H2 concentration.

Experimental Methodology

The research engine was run at 1200RPM for the best torque performance. An initial spark timing of 14 deg bTDC which resulted in a CA50 of 11 deg aTDC was selected for the preliminary set of tests, the SOI tests. A sweep of SOI timing tests was done with liquid LPG to evaluate the effect of closed (after IVC) and open valve (after IVO) port injection on performance, emissions, and combustion, and to select the optimal SOI for the rest of the study. With the optimal SOI determined, a spark timing sweep was carried out to establish the optimal combustion phasing, described as the MBT, with liquid LPG on the SCE. The effect of further advancing the spark timing past the MBT was also investigated to determine the effect of knock on the SCE. The MBT CA50 was then documented and utilized for the rest of the baseline study. The IMAP was increased from the naturally aspirated condition until a knock-limited load was achieved. Finally, the effect of equivalence ratio was explored from lean to rich engine operation regimes. The test matrix is presented in Table 2.

Table 2. Baseline test matrix.

ENGINE OPERATING PARAMETERS			
CR = 9.3:1, Manifold air temperature (MAT) = 38 deg C, Speed = 1200RPM, Injection pressure ~ 1.6MPa, Target BMEP ~ 900kPa			
SOI (deg bTDC)	Spark Timing (deg bTDC)	IMAP (kPa)	Equivalence Ratio
120, 150, 330, 360	6 – 18	100 – 140	0.83 – 1.25
Φ = 1 IMAP = 100kPa CA50 ~ 11 deg aTDC	SOI = 120 deg bTDC Φ = 1 IMAP = 100kPa	SOI = 120 deg bTDC Φ = 1 CA50 = MBT	SOI = 120 deg bTDC IMAP = 100kPa, CA50 = MBT
**SOI 120 and 360 deg bTDC were also evaluated at a knocking condition of CA50 = 3 deg aTDC	**The spark timing was advanced from 18 to 24 deg bTDC to investigate the occurrence and effect of knock		

Knock was quantified at all operating conditions using a time averaged method described in detail in previous literature [37 - 38]. The method applies a fast Fourier transforms (FFT) technique to the bandpass filtered in-cylinder pressure signal. The area bounded by the output, the FFT power spectrum amplitude, for 200 cycles is then defined as the knock integral (KI) in kPa^2. Equation 5 was used to calculate this KI in real time and this value was logged in LabView.

$$KI = KL(1) + KL(2) + KL(3) + \cdots + KL(n) \quad (5)$$

Where:

n = number of combustion cycles in the data set = 200

KL = knock amplitude at each combustion cycle, x

Heat release analysis was conducted using the single zone equation shown in Equation 6. The specific heat ratio, γ, was deduced in real-time by the LECM using the polytropic relation. The γ of compression was calculated from 30 deg bTDC to 10 deg bTDC and the γ of expansion was determined from 10 deg after the location of peak pressure to 60 deg after the location of peak pressure for that particular engine operating condition. The average of the compression and expansion γ was then used in Equation 6 to evaluate the apparent heat release rate (AHRR).

$$\frac{dQ}{d\theta} = \frac{\gamma}{\gamma - 1} P \frac{dV}{d\theta} + \frac{1}{\gamma - 1} V \frac{dP}{d\theta} \quad (6)$$

Where:

P is the in-cylinder pressure

Q is the heat release

V is the cylinder volume

Uncertainty analysis was performed in this paper by calculating the standard deviation (SD) of independent variables at each engine operating point. The data points used were ~3-minute averages (1000 consecutive cycles) for high-speed pressure data and ~2-minute averages for other independent variables. The root of summation of squares (RSS) technique shown in equation 7 was then applied to calculate the propagation of the SD from the independent variables to the results. However, only random errors were considered in this uncertainty analysis, as experiments were conducted on the same test cell over a relatively short period of time with the fixed errors assumed to be constant.

$$S_R = \left(\sum_{i=1}^{n} [S_{x_i} \frac{\partial R}{\partial x_i}]^2\right)^{1/2} \quad (7)$$

Where:

S_R is the total uncertainty of the result

S_{x_i} is the uncertainty of the independent variable x_i

The LPG tanks were filled at a local LPG supplier before the tests and the composition of the fuel was measured using a gas chromatograph. The composition of LPG used in this study and its properties are shown in Table 3.

Table 3. LPG properties.

Composition (%vol)	
Propane	98.473
Ethane	0.95
I-butane	0.49
N-butane	0.07
Propylene	0.01
Nitrogen	0.007
Properties	
LHV (MJ/kg)	46.36
H:C ratio	2.67
Stoichiometric AFR	15.57
Density (kg/m3)	493

Results and Discussion

Start of Injection (SOI)

The preliminary set of tests in this baseline evaluation were carried out to determine an optimal start of injection (SOI) timing. Figure 4 shows that 120 deg bTDC produced the highest brake torque, but there was no significant improvement in BTE between the closed intake valve injection SOI timings at 120 and 150 deg bTDC and the open intake valve SOI timings at 330 deg bTDC and 360 deg bTDC. Therefore, the optimal SOI that would be used in this study would mostly consider the combustion and emission characteristics at these injection timings.

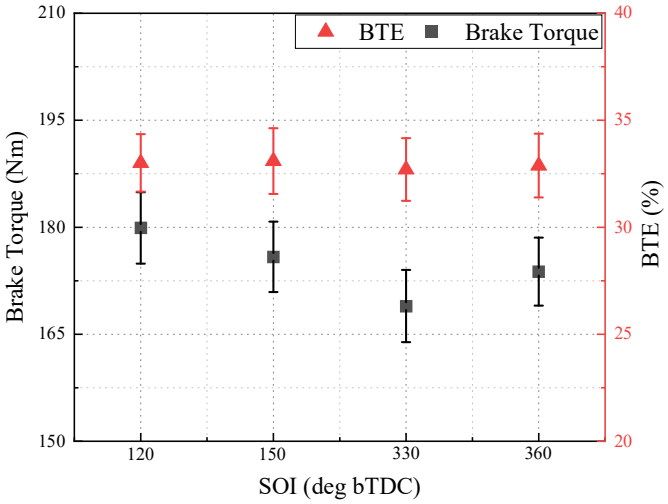

Figure 4. Brake Torque and BTE at open and closed valve injection timings.

The average in-cylinder pressure trace and apparent heat release rate indicated similar trends with the BTE. This trend is captured in Figure 5a. Further investigations were then conducted into the possible advantages of open valve timings over closed valve timings in the shape of charge cooling and its effect on knock. Spark timing was advanced to a knocking condition and the knock integral (KI) compared at this condition. Figure 5b presents the KI and COV of peak pressure, a measure of combustion stability, at the various injection timings. There was no observed difference in the knock integral values at all injection timings. However, the COV indicated that the close valve timing, 120 deg bTDC indicated a slightly more stable combustion at knocking conditions compared to open valve timing 360 deg bTDC. This is most likely due to the increased time for mixture preparation at closed valve injection timings and its promoting effect on the homogeneity of the fuel-air mixture entering the cylinder.

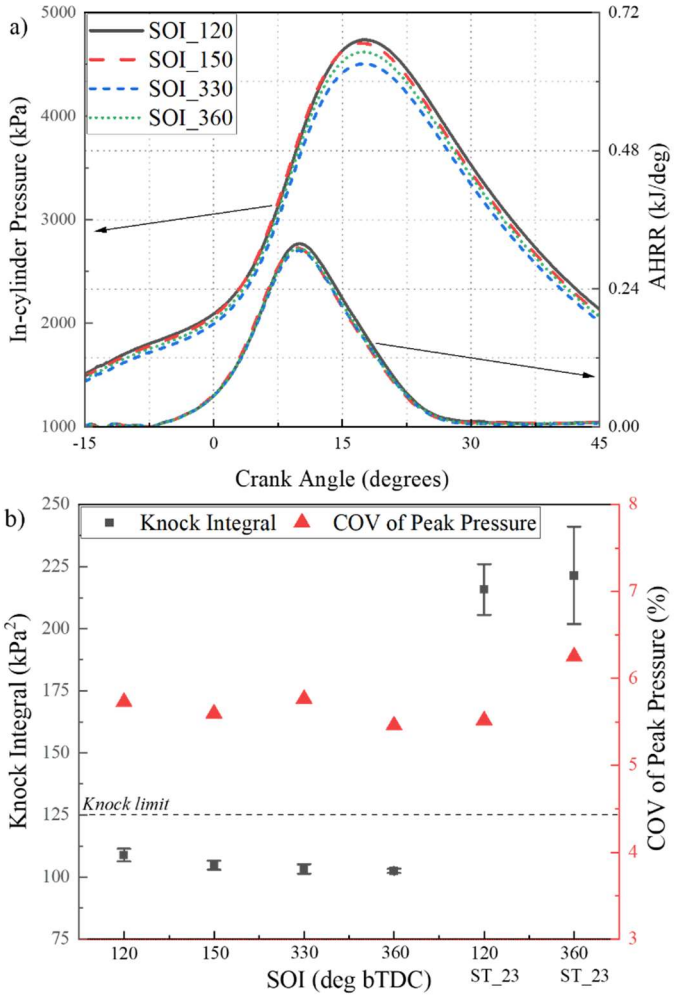

Figure 5. Comparison of (a) 1000-cycle averaged in-cylinder pressure trace and apparent heat release rates (b) knock integral and COV of peak pressure for all injection timings at knocking (spark timing 23 bTDC) and non-knocking conditions.

Finally, the engine-out emissions were compared to arrive at an optimal injection timing. The engine-out emissions were normalized with brake power and the brake specific results are plotted in Figure 6. In Figure 6a, the brake specific NOx remained fairly constant across the open and closed valve timings. The brake specific CO trends indicated a 6% increase in magnitude between the lowest value at closed valve timing 150 deg bTDC and at open valve timing 360 deg bTDC for non-knocking conditions, and a 10% increase between closed valve timing 120 deg bTDC and open valve timing 360 deg bTDC for knocking conditions. This CO increase was as a result of a greater degree of combustion incompleteness at the open valve timings possibly linked to mixture preparation time. In Figure 6b, while closed valve timing 150 deg bTDC indicated similar bsTHC and bsNMHC emissions to the open valve timing 330 deg bTDC, closed valve timing 120 deg bTDC produced the lowest bsTHC and bsNMHC at all non-knocking conditions. The closed valve timing (120 deg bTDC) producing the lowest hydrocarbon was similar to results presented by McGee et al. [39]. Therefore, owing to its slight advantage over the other timings especially in terms of brake torque, bsTHC and bsNMHC, 120 deg bTDC was selected as the optimal SOI for the rest of the baseline study.

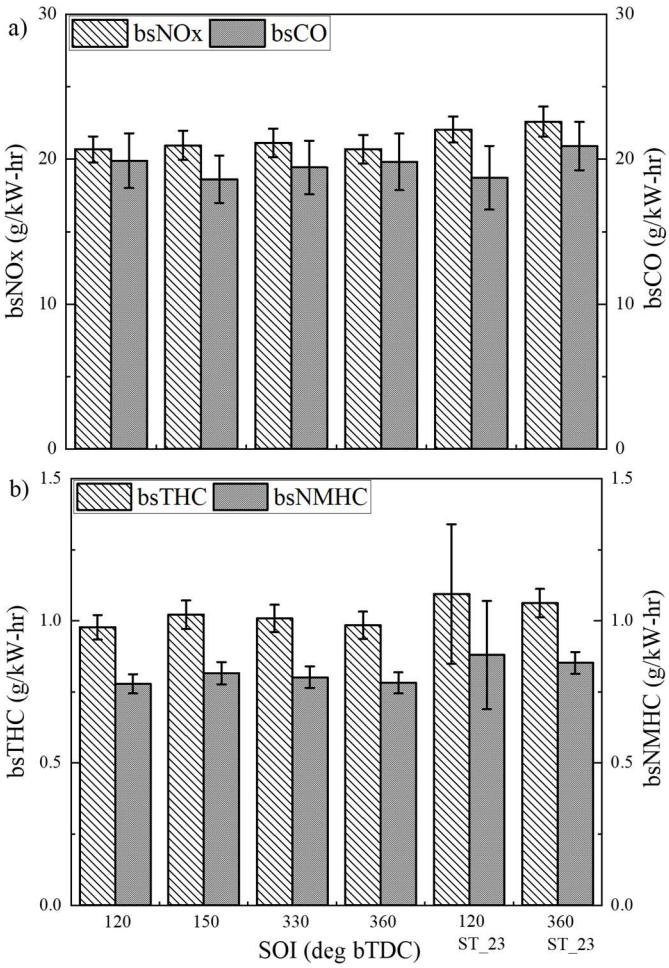

Figure 6. Brake power normalized engine-out (a) bsNOx and bsCO (b) bsTHC and bsNMHC, at the various start of injection timings and at knocking and non-knocking conditions.

Spark Timing

The MBT was determined by sweeping the spark timing from a retarded timing of 6 deg bTDC to more advanced timings at 18 deg bTDC. The spark timing that produced this ideal combustion phasing was determined and the corresponding 50% burn crank angle (CA50) was deduced and then, utilized for the rest of the study. In this study, brake torque, shown in Figure 7, was influenced by advancing the spark timing until an MBT was achieved at spark timing 16 deg bTDC corresponding to a CA50 of 9 deg aTDC. At this operating condition, the BTE was found to be 34%. Further tests on the engine also demonstrated this MBT value to be between CA50 9 and 11 aTDC. Previous studies by Sierens [40] determined this optimal combustion phasing to be slightly advanced between 7 and 8 deg aTDC, while Heywood [31] indicated that this value is typically at about 10 deg aTDC. The MBT is defined as the ideal combustion phasing where the work done by the combusting gas is minimized during compression and maximized during the expansion stroke. Therefore, for the rest of this study, an optimal combustion phasing was chosen to be CA50 10 deg aTDC to represent the average of MBTs demonstrated with liquid LPG PFI on the engine and maximize the engine performance.

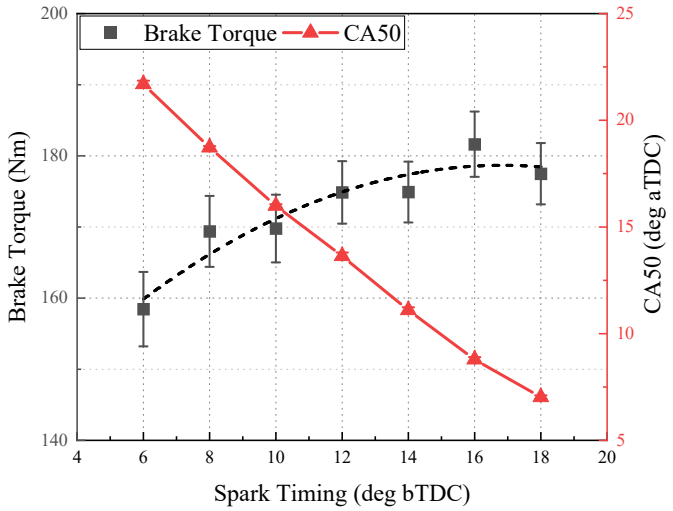

Figure 7. Demonstration of MBT combustion phasing at the investigated spark timings and corresponding CA50.

Figure 8 shows the average in-cylinder pressure traces and apparent heat release rates for the spark timing sweep. Figure 8a shows that the location of peak pressure approached TDC as the spark was advanced. The peak pressure also increased by 1.7MPa between spark timing 6 deg bTDC and 18 bTDC as a larger portion of the work performed by the combusting gases was done during the earlier part of the expansion stroke. The apparent heat release rates plot in Figure 8b present a slightly different trend where the maximum rate occurred at 16 deg bTDC, a consequence of the optimized combustion phasing. Further investigations were performed into the effect of advancing the spark timing beyond the MBT to determine the onset of knock and the knock integral trend with spark timing at the engine operating conditions. The spark timing was advanced to 24 deg bTDC and the results shown in Figure 8c. The knock integral was determined using the FFT method described earlier with a knock threshold determined at the operating conditions to be 125kPa^2. This determination was corroborated by an obvious change of slope on the apparent heat release rate curves which pointed to a secondary combustion event. The spark timing at which incipient knock was instigated was discovered to be at 20 deg bTDC corresponding to CA50 ~4 deg aTDC. The knock integral increased rapidly, indicating an exponential trend between spark timing 6 deg bTDC and the most advanced timing 24 deg bTDC. At this advanced combustion phasing, a significant portion of the combustion is occurring close to TDC at elevated pressures and temperatures, two factors that encourage end-gas autoignition.

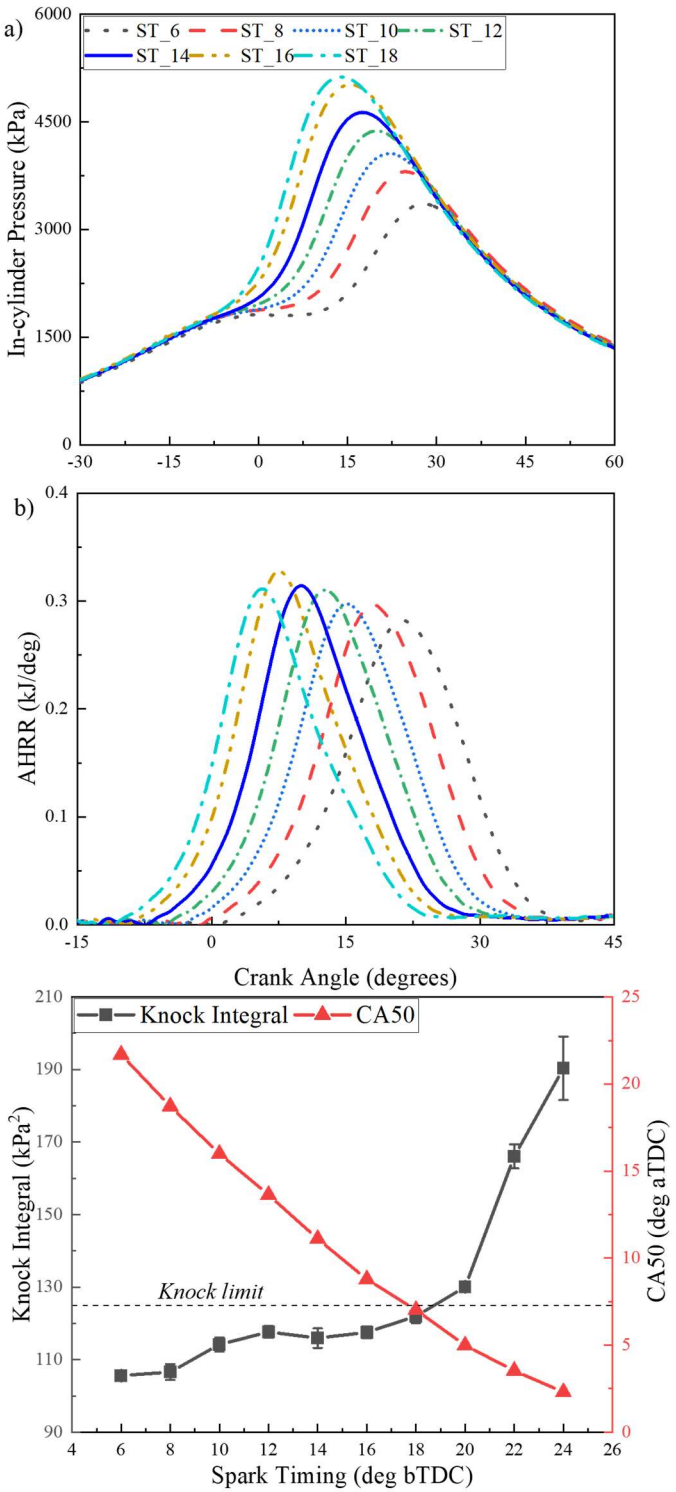

Figure 8. Combustion characteristics showing (a) 1000-cycle averaged in-cylinder pressure and (b) apparent heat release rates for spark timings 6 -18 deg bTDC (c) CA50 and knock integral for more advanced timings (6 – 24 deg bTDC).

The brake specific emissions are plotted in Figure 9. As spark timing was advanced, bsNOx, shown in Figure 9a increased marginally from 19.9g/kW-hr at 6 deg bTDC to 20.7g/kW-hr at 18 deg bTDC, while there was a decreasing bsCO trend with spark timing except for the outlier at spark timing 16 deg bTDC. The normalization by brake power was responsible for the marginal increase in bsNOx as NOx ppm values (not shown) increased significantly with advanced spark timing. This increasing NOx ppm trend was also observed in the literature [19, 40]. This uptick in NOx values is due to the increase in average in-cylinder temperatures which occurred as more of the combustion and heat release occurs closer to TDC. Figure 9b shows a more consistent and pronounced increase in bsTHC and bsNMHC as spark was advanced, corroborated by the findings of Wendeker et al [19]. This is likely due to the dual effect of increased in-cylinder pressure described earlier forcing more of the fuel-air mixture into the crevice volumes and, possibly to a larger extent, the effect of in-cylinder temperatures on the oxidation of HC. Retarded timings produce higher late-cycle temperatures as more of the combustion is happening later in the cycle. Therefore, as the hydrocarbon-air mixture that was pushed into the crevice volumes reenters into the combustion chamber, the higher temperatures at retarded timings cause more of the HC-air mixture to be oxidized.

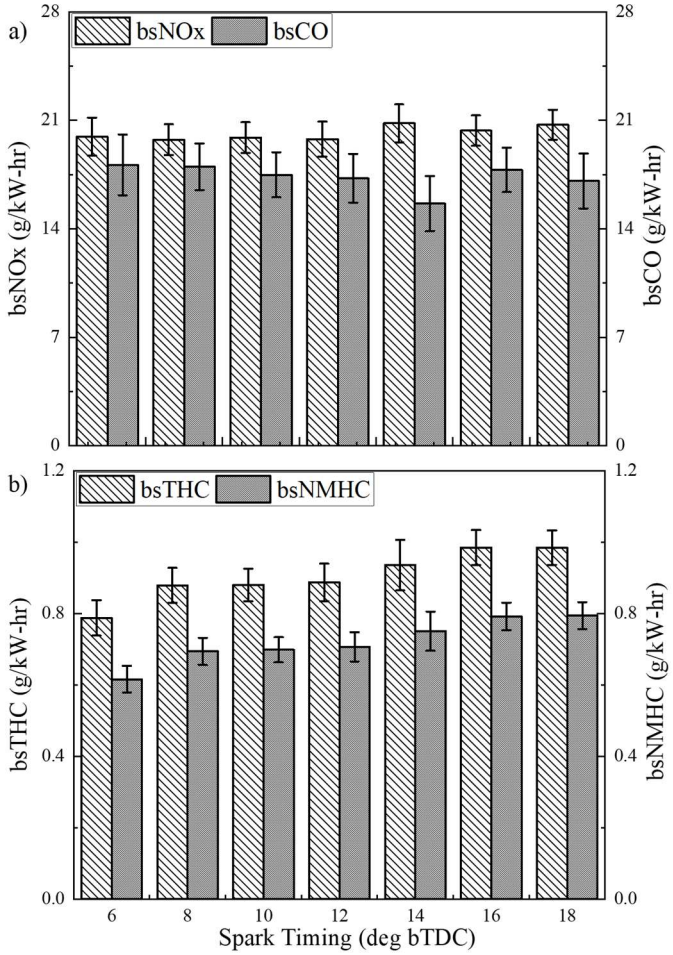

Figure 9. Comparison of engine-out emissions (a) bsNOx and bsCO (b) bsTHC and bsNMHC, for the spark timing sweep 6 -18 deg bTDC.

Intake Manifold Air Pressure (IMAP)

The load on the engine was increased from the initial 900kPa BMEP target, by increasing the IMAP, to a knocking operating condition. The knock limit was determined to be at an IMAP of 140kPa with a BMEP of ~1.3MPa. The results are presented in Figure 10. Two representative single cycle in-cylinder pressure traces at IMAP 100kPa and 140kPa along with their bandpass filtered values are plotted in Figure 10a. The pressure oscillations as a result of knocking combustion are visible on the IMAP 140kPa line. An increase of over 40% was recorded in peak pressure values between both operating conditions. The bandpass filtered pressure plots indicate the magnitude of the pressure oscillations observed at the increased load point of IMAP 140kPa. This represented >40%

increase compared to the IMAP 100kPa condition. Figure 10b shows the apparent heat release rate plots for each tested IMAP. The operating condition at IMAP 140kPa produced a maximum AHRR of ~0.45kJ/deg compared to 0.3kJ/deg at IMAP 100kPa as a result of the increased fuel mass required to maintain stoichiometry at the increased IMAP of 140kPa. A marked change in the AHRR slope at IMAP 140kPa was observed, which suggested the occurrence of a secondary combustion event and validated the determined knock limit [29]. The average peak pressure values are presented in Figure 10c. The trends described a steady linear rise in peak pressure values as IMAP was swept due to the increase in inducted fuel and air mass.

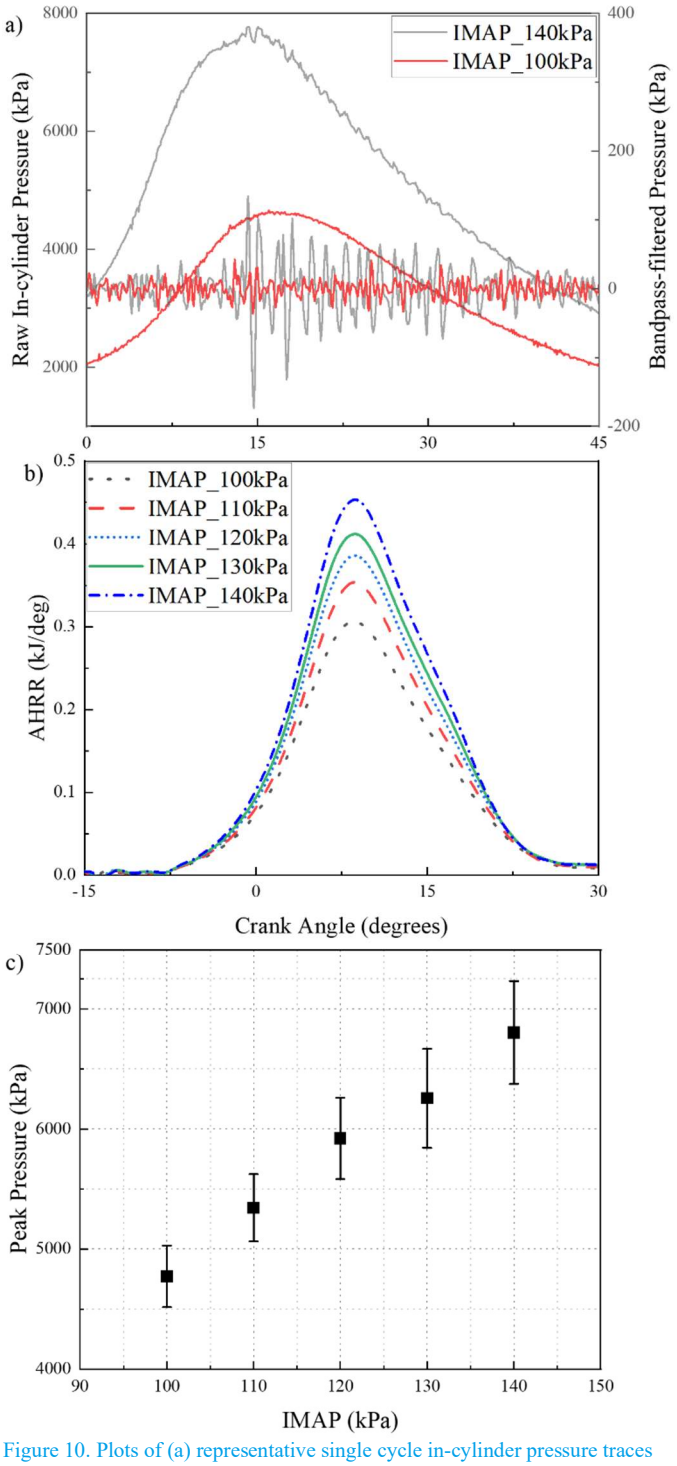

Figure 10. Plots of (a) representative single cycle in-cylinder pressure traces and bandpass filtered pressures at IMAP 100 and 140kPa (b) AHRR (c) peak pressure for a sweep of IMAP from 100kPa to the knock limit at 140kPa.

Figure 11 demonstrates the influence of increasing load on BTE and BSFC. As the amount of fuel and air inducted into the combustion chamber and the heat release rate increased with IMAP, a greater BTE was produced by the engine and an attendant reduction in BSFC was also observed. This desired trend was also observed in previous studies [41, 42]. The BSFC was reduced by over 5% to ~221g/kW-hr at the knocking condition of IMAP 140kPa. There was also a corresponding ~5% relative improvement in BTE as load was increased to the knock limit from the naturally aspirated conditions.

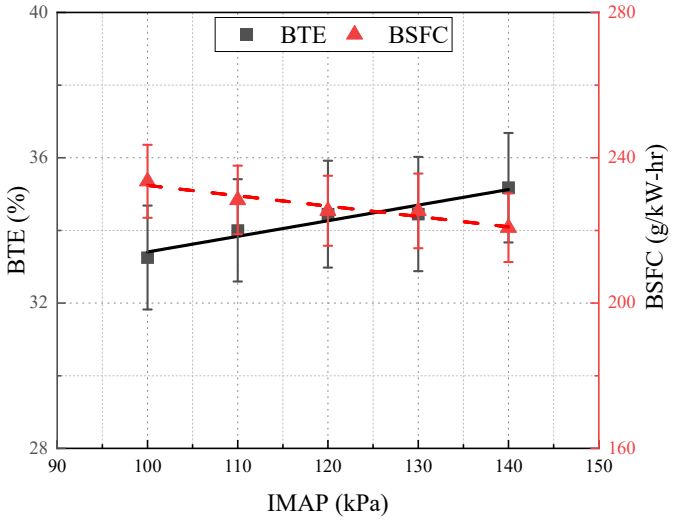

Figure 11. Plots of BTE and BSFC against IMAP at 1200RPM, φ = 1, MBT and MAT = 38 deg C.

The engine-out emissions are presented in Figure 12. The bsTHC decreased, as the load was increased, from 0.91g/kW-hr to 0.63g/kW-hr at the knock limit. This is similar to trends observed in previous studies [17,42]. Although, the crevice volume filling is expected to have a more pronounced effect on the bsTHC at the increased in-cylinder pressures shown previously, it is more likely that the competing effects of a more superior, complete combustion due to higher in-cylinder temperatures [42] and the normalization with larger brake powers at higher IMAPs combine to drive the bsTHC trend downwards. Similarly, it is believed that as load was increased, this normalization by larger brake powers contributed to the marginal reduction in bsNOx (20.3g/kW-hr at IMAP 100kPa to 19.5g/kW-hr at the knock limit) despite the increased in-cylinder temperatures.

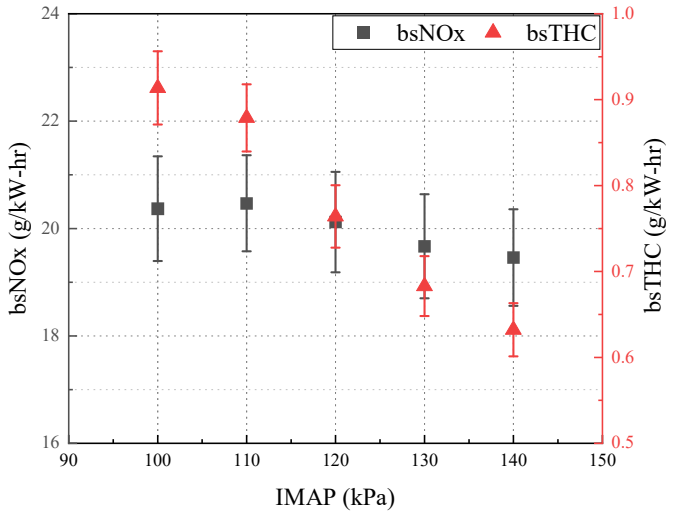

Figure 12. Comparison of engine-out bsNOx and bsTHC at all the investigated loads conditions on the engine.

Equivalence Ratio

Figure 13 shows the relationship between the brake torque, the BTE, and the equivalence ratio. The brake torque increased until an equivalence ratio just rich of stoichiometric at which point peak temperatures are typically experienced. Despite the relatively lesser brake torque values at the leanest operating condition (φ value of 0.83) investigated, the BTE was highest at this point, and this accounted for a ~22% relative improvement in BTE compared to the richest operating condition (φ value of 1.25). Several studies have also observed this trend of increasing efficiency with reducing equivalence ratio [18, 23, 31]. The BTE at lean conditions is higher due to the combustion products being at lower temperatures causing lower heat transfer and therefore, more expansion work to be extracted by the piston, while the at rich conditions the combustion inefficiencies from an overly rich mixture dominate [31] and this severely diminishes the BTE at these conditions.

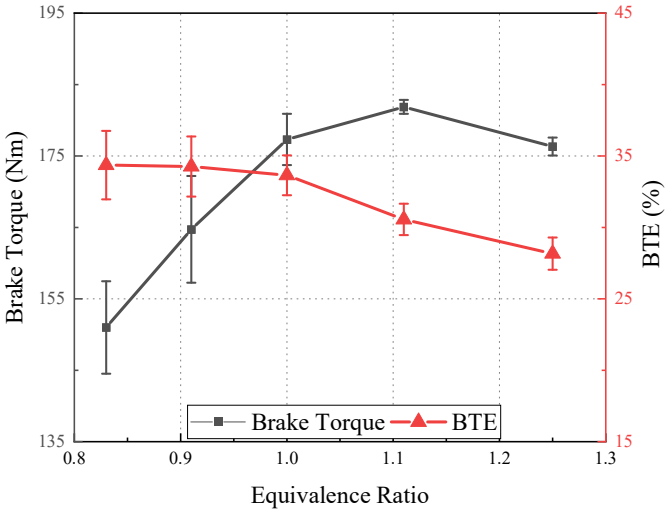

Figure 13. Comparison of brake torque and BTE for equivalence ratios 0.83 – 1.25 at engine operating condition: 1200RPM, IMAP - 100kPa, IMAT - 38 deg C and CA50 10 deg aTDC.

Combustion characteristics are presented in Figure 14. In Figure 14a, the COV of peak pressure, a measure of combustion stability, is plotted. For this metric, this study employed a limit of 10% to define an "unstable" engine operating condition. However, while all points were below this limit, the lean conditions were more unstable than the stoichiometric and rich conditions as evidenced in the plots. This is due to the charge dilution and reduced in-cylinder temperatures at lean conditions which results in reduced flame speed, longer burn durations and possible misfires. The burn durations (defined in this study as the time between a mass fraction burn (MFB) of 10% to a MFB of 90%) and ignition delays (defined as spark timing to MFB 10%) are shown in Figure 14b. Both the burn duration and ignition delay were reduced as the mixture was swept from lean to rich. Similar trends were captured by other researchers [4, 20]. The charge dilution and lower in-cylinder temperatures at lean conditions is also responsible for this observation. Figure 14c shows the apparent heat release rates and in-cylinder pressures for all the tested equivalence ratios. The key observations were, the longer crank angle duration required for heat release at equivalence ratio 0.83, again due to the reduced flame speed and lower temperatures, and that equivalence ratio 1.11 indicated the shortest duration of heat release and the maximum in-cylinder pressure. This is consistent with literature [31] and is due to the fact that the maximum in-cylinder temperatures are expected just rich of stoichiometric, typically at equivalence ratio 1.1.

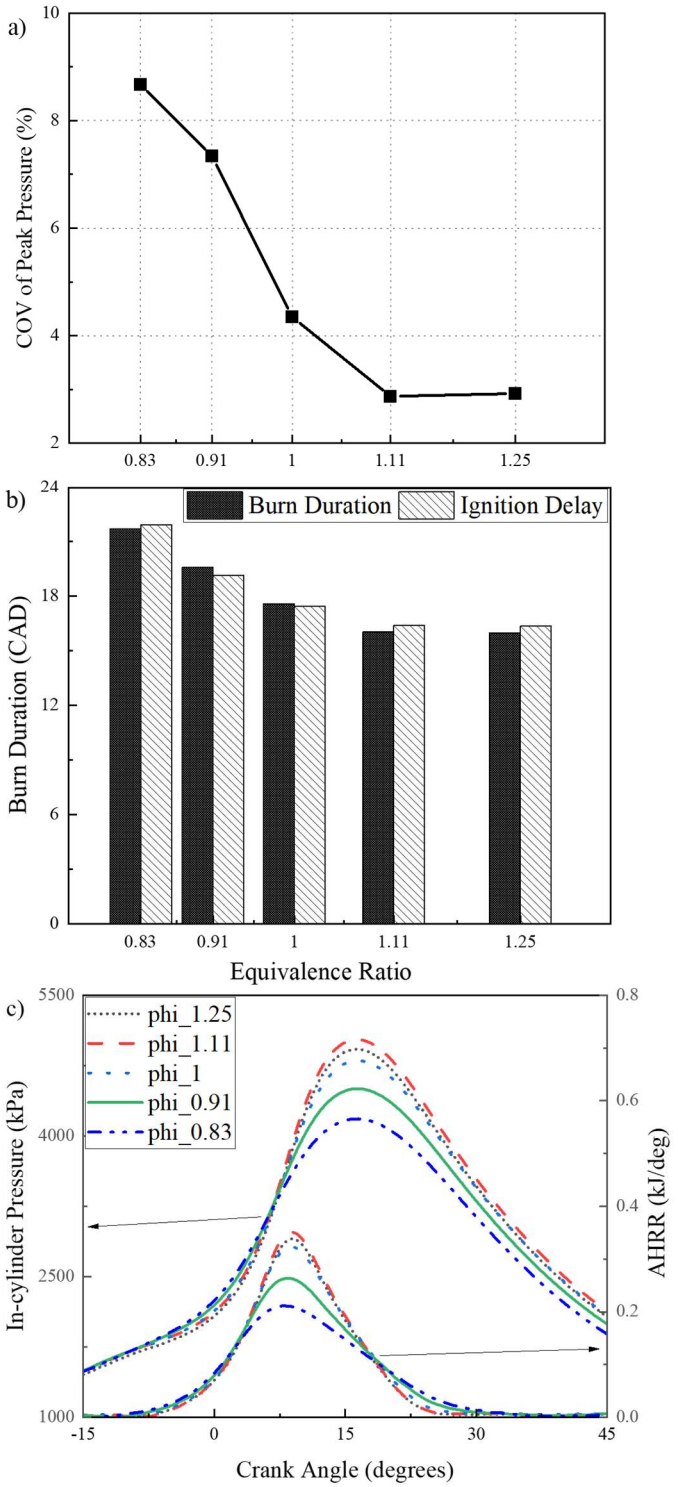

Figure 14. Combustion parameters (a) COV of peak pressure (b) burn duration and ignition delay (c) 1000-cycle averaged in-cylinder pressure and AHRR for the sweep of equivalence ratios at engine operating conditions 1200RPM, CA50 10 deg aTDC, IMAP 100kPa and MAT 38 deg C.

Figure 15a shows the dependence of bsCO and $bsCO_2$ on equivalence ratio. At rich conditions, there is insufficient oxygen for complete oxidation and as such the bsCO was exponentially higher compared to the really low values at lean conditions where a 99% reduction in bsCO was recorded. Similar trends were observed in previous studies [18, 23, 31]. The CO_2 raw percentages followed the trends described by Heywood [31], peaking at stoichiometry and reducing on either side. However, the effect of brake power normalization is visible in the plots as the peak $bsCO_2$ is observed at slightly lean conditions. In Figure 15b, the bsNOx increased as the mixture was leaned out, peaked at 0.91 and began to drop at 0.83. This trend can be described by the competing effects of available oxygen and in-cylinder temperatures. At rich conditions, there is not enough available oxygen for the formation of NOx despite the high in-cylinder temperatures, hence the lower values of bsNOx made lower still by the normalization with larger brake power numbers. At the lean condition, 0.91, temperatures are low enough to discourage NOx formation but the available oxygen from the abundant air encourages the formation of NOx. At the leaner condition of 0.83, the effect of the again reduced in-cylinder temperatures dominated and the bsNOx values began to reduce. An important class of regulated emissions in LPG SI engines are the HC and NMHC and these values are also shown in Figure 15b. There was a slight drop in these emissions between 0.83 and 0.91, and then a significant rise at richer conditions. The HC trends were also observed by previous studies [18, 23, 31].

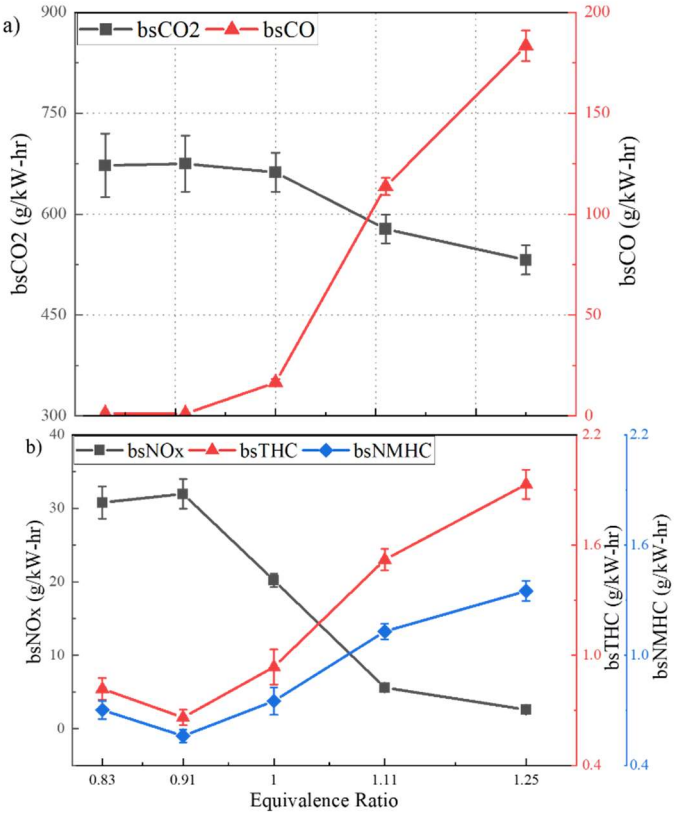

Figure 15. Brake specific engine-out emissions (a) bsCO2 and bsCO (b) bsTHC, bsNOx, bsNMHC, bsNMNEHC against equivalence ratio.

Summary/Conclusions

This study presented the development of a liquid phase port-injection system for LPG on a heavy-duty single cylinder engine, the design of a 9.3:1 compression ratio piston to replicate the performance of selected current LPG engines, and the baseline evaluation of the performance, combustion, and emissions characteristics to establish a benchmark comparable to existing LPG engines. The experimental results showed that:

- The PFI system consistently delivered liquid LPG at an injection pressure of 1.6MPa. This set-up guaranteed excellent control of the combustion and air-fuel ratio during the baseline experiments.
- An optimal SOI was determined by investigating the effect of open and closed valve injection timings on the engine. The closed valve timing, 120 deg bTDC, produced the lowest bsTHC and bsNMHC emissions. There was no significant improvement in BTE and knocking intensity across the injection timings. At knocking conditions, combustion stability was slightly improved by the closed valve timing, 120 deg bTDC, which also produced 10% lower bsCO than the open valve timing, 360 deg bTDC. 120 deg bTDC was selected as the optimal SOI for this study.
- The ideal combustion phasing, represented as the MBT was determined to be between CA50 9 - 11 deg aTDC. The BTE using the ideal combustion phasing on this SCE was 34%, a 3% improvement over the most retarded timing with CA50 21 deg aTDC. The occurrence of incipient knock was found to correspond to a CA50 around 4 deg aTDC.
- The engine exhibited knocking combustion at a BMEP of 1.3MPa, corresponding to an IMAP of 140kPa. This operating condition indicated a 40% increase in peak pressure, ~5% relative improvement in BTE and over 5% reduction in BSFC compared to the naturally aspirated condition.
- At the increased load point, the bsTHC reduced from 0.91g/kW-hr to 0.63g/kW-hr, the bsNOx indicated a slight reduction as well while the maximum rate of apparent heat release increased by 33% from 0.3kJ/deg to 0.45kJ/deg.
- There was a 6% increase in BTE between the lean condition at equivalence ratio 0.83 (34.4%) and the rich condition at equivalence ratio 1.25 (28.2%).
- The slightly lean condition at equivalence ratio 0.91, accounted for the greatest bsNOx values but produced a 66% reduction bsTHC emissions compared with the richest condition. There was also a sharp reduction in bsCO as the mixture was leaned out, with over 99% of the bsCO produced at the rich operation condition unaccounted for at lean conditions.
- Finally, the baseline LPG BTE on the heavy-duty engine platform was established as 34% i.e., at naturally aspirated, MBT, and stoichiometric conditions with PFI LPG.

References

1. U.S. Energy Information Administration (EIA)., "Use of energy for transportation," Retrieved October 11, 2022, from https://www.eia.gov/energyexplained/use-of-energy/transportation.php.
2. Bae, C., and Kim, J., "Alternative Fuels for Internal Combustion Engines," Proceedings of the Combustion Institute, 36(3), 3389–3413, 2017, https://doi.org/10.1016/j.proci.2016.09.009.
3. Kalghatgi, T., The Outlook for Fuels for Internal Combustion Engines," International Journal of Engine Research, Vol. 15, Issue 4, pp. 383–398, 2014, SAGE Publications Ltd, https://doi.org/10.1177/1468087414526189.
4. Campbell, M., Wyszyński, P., and Stone, R., "Combustion of LPG in a Spark-Ignition Engine," SAE Transactions (Vol. 113), 2004.
5. Gomez, E., Walker, B., "National Propane Survey 2017 – 2018 Final Report," Southwest Research Institute, San Antonio, TX. Prepared for Propane Education and Research Council, Docket No. 21257, SWRI Project No. 08.23448, 2019.
6. Fosudo, T., Kar, T., Marchese, A., Windom, B. et al., "The Impact of LPG Composition on Performance, Emissions, and Combustion Characteristics of a Pre-mixed Spark-Ignited CFR Engine," SAE Technical Papers 2022-01-0476, 2022, https://doi.org/10.4271/2022-01-0476.
7. Saleh, E., "Effect of Variation in LPG Composition on Emissions and Performance in a Dual Fuel Diesel Engine," Fuel 87, no. 13-14 (2008): 3031-3039, 2008, doi:10.1016/j.fuel.2008.04.007.
8. Kar, T., Fosudo, T., Slunecka, C., Marchese, A. et al, "A Study of Propane Combustion in a Spark-Ignited Cooperative Fuel Research (CFR) Engine," SAE Technical Paper 2022-01-0404, 2022, https://doi.org/10.4271/2022-01-0404.
9. Krieck, M., Günther, M., Pischinger, S., Kramer, U. et al, "Effects of LPG Fuel Formulations on Knock and Pre-Ignition Behavior of a DI SI Engine," SAE International Journal of Engines, 9(1), 237–251, 2015, https://doi.org/10.4271/2015-01-1947.
10. Boretti, A., and Watson, C., "Development of a Direct Injection High Efficiency Liquid Phase LPG Spark Ignition Engine," SAE Int. J. Engines, Vol 2(1), 1639-1649, 2009.
11. Lasocki, J., Kopczynski, A., Krawczyk, P., and Roszczyk, P., "Empirical Study on the Efficiency of an LPG-supplied Range Extender for Electric Vehicles," Energies, 12(18), 2019, https://doi.org/10.3390/en12183528.
12. Nutu, C., Pana, C., Negurescu, N., and Cernat, A. et al., "LPG as a Fuel for Diesel Engines-Experimental Investigations," IOP Conference Series: Materials Science and Engineering, 252(1), 2017, https://doi.org/10.1088/1757-899X/252/1/012079.
13. Boretti, A., "Advantages and Disadvantages of Diesel Single and Dual-Fuel Engines," Frontiers in Mechanical Engineering (Vol. 5), 2019, https://doi.org/10.3389/fmech.2019.00064.
14. Leermakers, J., van den Berge, B., Luijten, M., de Goey, H. et al., "Direct Injection of Diesel-Butane Blends in a Heavy-Duty Engine," SAE International Journal of Fuels and Lubricants, 4(2), 179–187, 2011, https://doi.org/10.4271/2011-01-2400.
15. Cinar, G., Eldamanhory, A., Akansu, O., Enes Fil, H. et al., "Experimental Study on an SI Engine Fueled By LPG/Acetylene Mixtures," International Journal of Automotive Technology, 21(5), 1323–1331, 2020, https://doi.org/10.1007/s12239-020-0125-5.
16. Masi, M., and Gobbato, P., "Measure of the Volumetric Efficiency and Evaporator Device Performance for a Liquefied Petroleum Gas Spark Ignition Engine," Energy Conversion and Management, 60, 18–27, 2012, https://doi.org/10.1016/j.enconman.2011.11.030.
17. Watson, C., and Phuong, X., "Why Liquid Phase LPG Port Injection has Superior Power and Efficiency to Gas Phase Port Injection," SAE Technical Paper 2007-01-3552, 2007, https://doi.org/10.4271/2007-01-3552.
18. Pradeep, V., Bakshi, S., and Ramesh, A., "Direct Injection of Gaseous LPG in a Two-Stroke SI Engine for Improved Performance," Applied Thermal Engineering, 89, 738–747, 2015, https://doi.org/10.1016/j.applthermaleng.2015.06.049.
19. Wendeker, M., Jakliński, P., Czarnigowski, J., Boulet, P. et al., "Operational Parameters of LPG Fueled SI Engine-Comparison of Simultaneous and Sequential Port Injection," SAE International, 2007-01-2051, 2007.
20. Pradeep Bhasker, J., and Porpatham, E., "LPG Gaseous Phase Electronic Port Injection on Performance, Emission and Combustion Characteristics of Lean Burn SI Engine," IOP Conference Series: Earth and Environmental Science, 40(1), 2016, https://doi.org/10.1088/1755-1315/40/1/012069.
21. Tukiman, M., Mustaffa, N., Fawzi, M., Osman, A. et al., "A Comparative Study of an LPG-Spark Ignition Engine using Liquid Sequential Injection Technique, MATEC Web of Conferences, 78, 01050, 2016, https://doi.org/10.1051/01050.
22. Park, C., Oh, S., Kim, T., Oh, H. et al., "Combustion Characteristics of Stratified Mixture in Lean-Burn Liquefied Petroleum Gas Direct-Injection Engine with Spray-Guided Combustion System," Journal of Engineering for Gas Turbines and Power, 138(7), 2016, https://doi.org/10.1115/1.4031876.
23. Dube, A., Vivekanand, M., and Ramesh, A., "Experimental Studies on Liquid Phase LPG Direct Injection on a Two-Stroke SI Engine," SAE International Journal of Engines, 12(3), 2019, https://doi.org/10.4271/03-12-03-0023.
24. Kar, T., Fosudo, T., Windom, B., Olsen, D. et al., "Development of a Liquid-Phase LPG Delivery System for Direct Injection, Spark-Ignited Engines," Proceedings of the ASME ICEF conference, 2022.
25. Tuan, T., and Dong, P., "Theoretical and Experimental Study of an Injector of LPG Liquid Phase Injection System," Energy for Sustainable Development, 63, 103–112, 2021, https://doi.org/10.1016/j.esd.2021.06.002.
26. Barroso, M., Ribas, X., Pita, M., Dominguez, J. et al., "HD Diesel Engines Development for Alternative Fuel Use," SAE International Journal of Engines, 8(1), 326–340, 2015, https://doi.org/10.4271/2015-26-0056.
27. Zdanowicz, A., Mohr, J., Bestel, Diego., Rueda, F. et al., "Expanding the Knock/Emissions/Misfire Limits for the Realization of Ultra-Low Emissions, High Efficiency Heavy Duty Natural Gas Engines". United States, 2021, https://doi.org/10.2172/1828241.
28. Olsen, D., and Kirkpatrick, A., "Experimental Examination of Prechamber Heat Release in a Large Bore Natural Gas Engine." Journal of Engineering for Gas Turbines and Power, 130(5), 2008, https://doi.org/10.1115/1.2906182.
29. Rodriguez, F., Xu, H., Hampson, G., Windom, B. et al., "Heavy Duty Natural Gas Single Cylinder Research Engine Installation, Commissioning, and Baseline Testing," Energy and Power Engineering, 14, 217-232, 2022, https://doi.org/10.4236/epe.2022.146012.
30. Olsen, D., Marchese, A., Windom, B., Xu, H. et al., "Development of Advanced Combustion Strategies for Direct Injection Heavy duty LPG Engines to Achieve Near-Diesel Engine Efficiency," Colorado State University Control Number: 2197-2095, 2020.
31. Heywood, J.B., "Internal Combustion Engine Fundamentals," McGraw-Hill, New York, USA, 1988.
32. Kar, T., Fosudo, T., Marchese, A., Windom, B. et al., "Effect of Fuel Composition and EGR on Spark-Ignited Engine Combustion with LPG Fueling: Experimental and Numerical

Investigation," Fuel 327, 2022, https://doi.org/10.1016/j.fuel.2022.125221.
33. Mizushima, N., Sato, S., Ogawa, Y., Yamamoto, T. et al., "Combustion Characteristics and Performance Increase of an LPG-SI Engine with Liquid Fuel Injection System," SAE International, 2009-01-2785, 2009.
34. Kim, Y., Lee, Y., Kim, C., and Shin, M., "Effects of Shape and Surface Roughness on Icing and Condensation Characteristics of an Injector in a Liquid Phase LPG Injection System," Fuel, 132, 82–92, 2014, https://doi.org/10.1016/j.fuel.2014.04.010.
35. Battino, R., Rettich, R., and Tominaga, T., "The Solubility of Nitrogen and Air in Liquids," Journal of Physical and Chemical Reference Data, 13(2), 563–600, 1984, https://doi.org/10.1063/1.555713.
36. Urban, C., and Sharp, C., "Computing Air/Fuel Ratio from Exhaust Composition," Natural Gas and Alternative Fuels for Engines ASME 1CE-Vol. 24, 1994.
37. Wise, M., Olsen, D., Kim, M., "Development of A Lean Burn Methane Number Measurement Technique for Alternative Gaseous Fuel Evaluation," Proc. ASME. ICEF2013, 2: Fuels; Numerical Simulation; Engine Design, Lubrication, and Applications, V002T02A014, 2014, doi.org/10.1115/ICEF2013-19220.
38. Bayliff, S., Olsen, D., Windom, B., Baker, D., "Evaluation of Controlled End Gas Auto-Ignition with Exhaust Gas Recirculation in a Stoichiometric, Spark Ignited, Natural Gas Engine," Colorado State University, Mechanical Engineering; Thesis, 2020.
39. McGee, M., Curtis, W., Russ, G., Lavoie, A., "The Effects of Port Fuel Injection Timing and Targeting on Fuel Preparation Relative to a Pre-Vaporized System," SAE Technical Paper 2000-01-2834, 2000.
40. Sierens, R., "An Experimental and Theoretical Study of Liquid LPG Injection," SAE Technical Paper 922363, 1992, https://doi.org/10.4271/922363.
41. Fosudo, T., Kar, T., Windom, B., and Olsen, D., "Comparative Analysis of a Spark-Ignited CFR Engine Operation on Compressed Natural Gas and Liquefied Petroleum Gas at Stoichiometric Conditions," Proceedings of the Western States Section of the Combustion Institute Spring Technical Meeting, 2022.
42. Singh, S., Dhar, A., and Agarwal, A., "Technical feasibility study of butanol-gasoline blends for powering medium-duty transportation spark ignition engine," Renewable Energy, 76, 706–716, 2015, https://doi.org/10.1016/j.renene.2014.11.095.

Contact Information

Toluwalase Fosudo,

toluwalase.fosudo@colostate.edu

fosudotolu@yahoo.com

Acknowledgments

This material is based upon work supported by the U.S. Department of Energy's Office of Energy Efficiency and Renewable Energy (EERE) under award number DE-EE0009198.

Definitions/Abbreviations

AFR	Air-Fuel Ratio
AHRR	Apparent Heat Release Rate
aTDC	After Top Dead Center
bTDC	Before Top Dead Center
BMEP	Brake Mean Effective Pressure
BS	Brake Specific
BSFC	Brake Specific Fuel Consumption
BTE	Brake Thermal Efficiency
CA50	50% Burn Crank Angle
CFR	Cooperative Fuel Research
CNG	Compressed Natural Gas
CO	Carbon Monoxide
COV	Coefficient of Variation
CR	Compression Ratio
DI	Direct Injection
EGR	Exhaust Gas Recirculation
EOI	End Of Injection
EVC	Exhaust Valve Closing
EVO	Exhaust Valve Opening
FFT	Fast Fourier Transform
HC	Hydrocarbons
IMAP	Intake Manifold Air Pressure
IVC	Intake Valve Closing
IVO	Intake Valve Opening
KI	Knock Integral
LECM	Large Engine Control Module
LPG	Liquefied Petroleum Gas
LSI	Liquid Sequential Injection

MAT	Manifold Air Temperature	**SCE**	Single Cylinder Engine
MBT	Maximum Brake Torque	**SI**	Spark Ignited
MFB	Mass Fraction Burned	**SOI**	Start Of Injection
NMHC	Non-Methane Hydrocarbons	**TDC**	Top Dead Center
NMNE	Non-Methane Non-Ethane	**THC**	Total Hydrocarbons
NOx	Oxides of Nitrogen		
PFI	Port Fuel Injection		
RON	Research Octane Number		